Lithium transition metal (Ti, Nb, V) oxide mesoporous thin films: contrasting results when attempting direct synthesis by evaporation-induced self assembly

S. Caes[a], C. Malherbe[b], N. Krins[a], J.C. Arrebola[a], C. Henrist[a], R. Cloots[a], B. Vertruyen[a,*]

[a] LCIS/GREENMAT, Department of Chemistry, Chemistry Institute B6, University of Liège, 4000 Liège, Belgium
[b] Laboratoire de Chimie Analytique Inorganique, Department of Chemistry, Chemistry Institute B6, University of Liège, 4000 Liège, Belgium
*corresponding author - phone +3243663452, fax +3243663413, b.vertruyen@ulg.ac.be

Abstract

This work investigates the possibility to prepare mesoporous thin films of Li-Ti, Li-Nb, Li-Nb-V and Li-V oxides through a direct sol-gel EISA route by dissolving a lithium salt in the precursor solution. Experimental conditions involve a hydrolysis molar ratio H_2O/TM ~10 (TM = Ti,Nb,V) and the common Pluronic structuring agent P123 (EO_{20}-PO_{70}-EO_{20}). Systematic formation of lithium-containing oxides as first-crystallizing phases points to a significant intermixture of lithium and transition metal ions in the inorganic network. In the case of Ti-based and Nb-based oxide films, addition of lithium to the precursor solution is compatible with the formation of amorphous mesoporous films at 350°C. On the contrary, addition of lithium has a detrimental effect on the notoriously difficult formation of vanadium-based mesostructured films: even when replacing half of the vanadium by niobium as a stabilizer, formation of mesostructured films has not been possible in the investigated range of experimental conditions.

Keywords
Mesoporous thin films; lithium transition metal oxides; soft-templating; EISA

1. Introduction

When seeking to improve the electrochemical performances of electrodes in Li-ion batteries, a flourishing approach is to favour architectures featuring a high contact area between electrode material and electrolyte. In this respect, mesoporous thin films are attractive electrodes for microbatteries [1] because they offer high specific area, interconnected porosity, homogeneous pore size and nanoscale wall thickness.

Evaporation-induced self-assemby (EISA) [2,3] is a well-known method to produce mesoporous thin films through sol-gel chemistry combined with soft-templating by amphiphilic block copolymers. When considering microbatteries, insertion of lithium in mesoporous thin film electrodes can be devised in two ways: (i) the usual approach is electrochemical insertion into the mesoporous transition metal oxide during battery cycling; (ii) another approach is the direct synthesis of the mesoporous lithium transition metal oxide thin film by addition of a lithium salt into the sol-gel precursor solution.

This latter approach used to be disregarded due to postulated difficulties concerning the condensation of the inorganic network and the interactions of the transition metal and the lithium ions with the ethylene oxide block of the surfactant [4-9]. However, Haetge et al. [10] have recently reported the synthesis of $Li_4Ti_5O_{12}$ mesoporous thin films by an EISA route. This experiment was conducted with a low hydrolysis molar ratio (i.e., water was supplied

only through the controlled relative humidity), using a structure directing agent with high decomposition temperature (KLE - poly(ethylene-co-butylene)-block-poly(ethylene oxide)).

In the present study, we have investigated the possibility to use the "direct synthesis" approach for several mesoporous lithium transition metal oxide thin films, using a typical hydrolysis molar ratio H_2O/TM ~10 and the common P123 (EO_{20}-PO_{70}-EO_{20}) Pluronic structuring agent. For each transition metal (Ti, Nb, V), the lithium/transition metal molar ratio was varied from 0 to 1. Titanium, niobium and vanadium transition metals were selected because all of them form oxide phases that are able to reversibly insert lithium [11-13], while the synthesis of the lithium-free oxides mesoporous thin films by EISA is increasingly difficult in the series Ti – Nb – V. On the one hand, titanium and niobium are well-known to form mesoporous structures quite easily [14,15]. On the other hand, vanadium is much more troublesome, due to its various oxidation states and reluctance of V^{5+} species to achieve adequate curvature [4]. Combining Nb and V makes it easier to obtain mesoporosity [13,16]. Comparison of the different cases is expected to provide insight into the consequences of lithium addition in the sol-gel solution.

For each composition, the presence of mesoporosity was checked by transmission electron microscopy and atmospheric ellipsometry porosimetry (Section 3.3). The decomposition of the structuring agent (Section 3.2) and the structure of the inorganic network (Section 3.4) were investigated by infrared spectroscopy, Raman spectroscopy and grazing-incidence X-ray diffraction.

2. Experimental

Thin films of various compositions were prepared by the dip coating method with P123 (EO_{20}-PO_{70}-EO_{20}, Sigma Aldrich) as the structuring agent for the EISA mechanism. In a typical experiment, dissolution of P123 in ethanol (analytical reagent grade, Fisher Chemical) was followed by addition of appropriate amounts of solid LiCl (p.a., Merck), liquid $Ti(OC_3H_7)_4$ (98+%, Acros Organics), 0.9 mol/l solution of $NbCl_5$ (99.95%, Alfa Aesar) in ethanol and/or 0.9 mol/l solution of VCl_4 (99+%, Acros Organics) in ethanol. Finally, hydrolysis of the precursor solutions was triggered by addition of distilled water for Nb-, NbV- and V-based solutions or HCl (37 wt.%, p.a., Merck) in the case of the Ti-based solutions. Synthesis flowcharts and concentrations of all species in the precursor solutions can be found in Supplementary Information 1 (SI-1). Rectangular substrates were cut from single crystal (001) silicon wafers (purchased from Silicium Materials) and submitted to surface oxidation in nitric acid overnight. During the dip coating procedure, the substrates were withdrawn from the precursor solutions at 2 mm/s in a constant relative humidity of 20%. All films were then heated at 200°C for one hour prior to heat treatment to higher temperature (see 'Results and discussion' section).

All films are labelled according to the following code: xTM-yLi-zEO where TM is the chemical symbol of the transition metal, Li is lithium, EO stands for an ethylene oxide unit in P123 and x, y and z represent relative molar ratios of TM, Li and EO in the precursor solution.

Some precursor solutions were characterized by dynamic light scattering (Viscotek 802 DLS) and/or UV-Visible spectroscopy (Perkin Elmer lambda 14P, 1 cm-long PMMA cuvettes, 300-1000 nm spectral range). Infra-red spectra were recorded by transmission on films coated on silicon substrates using a Bruker Equinox 55. A Jobin-Yvon Labram Raman spectrometer (laser wavelength 632.8 nm) was used to characterize fragments scratched from the films and deposited on a stainless steel substrate. X-ray diffractograms (XRD) were collected using a Bruker D8 grazing incidence diffractometer with Cu K_{alpha} radiation. Transmission electron micrographs (TEM) of fragments scratched from the films were obtained in a TECNAI G2 TWIN (LaB6, 200 kV). Film thickness was determined by

ellipsometric spectroscopy performed in the visible spectral range (1.23-3.00 eV) with a SOPRALAB GES-5E instrument. In addition to the optical thickness determination, an atmospheric porosimeter module was used to determine the open porosity of the sample. Data treatments were performed with the *WinElli II* software (SOPRALAB). A Cauchy law was sufficient to fit the experimental curves for thickness and refractive index *n* determination. Then, variations of the index *n* according to water partial pressure P/P_0 in the porosimeter module were used to plot the isotherm curves (absorption and desorption branches). The Lorentz-Lorenz effective medium model, corresponding in the present case to a mixture of void (pores) and material, was applied in order to calculate the water volume filling the pores and deduce the relative open-porosity value. The derivation of the absorption/desorption branch according to the Kelvin equation [17] provided the pore size distribution (PSD).

3. Results and discussion

3.1. Formation of hybrid films

For each transition metal (Ti, Nb, V) or combination of transition metals (NbV), precursor solutions were prepared with lithium/transition metal molar ratio varying from 0 to 1 (see SI-1 for concentrations of all species). Increasing the lithium content in the precursor solutions leads to a higher cationic concentration, which results in an increase of the viscosity (e.g., from 10.0 cP for the 1Ti-0Li-1EO solution to 16.5 cP for the 1Ti-1Li-1EO solution) and a larger volume of solution adhering to the substrate during dip coating.

The solvent of the inorganic precursors and P123 structuring agent is a mixture of ethanol and water with ethanol:water weight ratio of 93:7 (85:15 in the case of titanium-based solutions). The P123 content represents 5.8 wt% of the water+ethanol+P123 mass (16 wt% in the case of titanium-based solutions). In such conditions, no micelle formation is detected by dynamic light scattering experiments, in agreement with the water-ethanol-P123 phase diagrams reported in [18] and [19]. Since the concentration of P123 structuring agent is below the critical micellar concentration, micelle formation occurs only after dip coating, due to the increase in P123 concentration driven mainly by ethanol evaporation.

It is well-known that the organization of the hybrid phase obtained through such Evaporation-Induced Self-Assembly (EISA) mechanism depends on a number of experimental conditions [20]. In particular, formation of lamellar, hexagonal or cubic mesostructures (depending on the volume fraction of the structuring agent [21]) usually requires aging of the as-deposited film at room temperature, often in high relative humidity (RH), in order to ensure sufficient flexibility of the mesophase. On the contrary, in the present work dip coating was carried out in low relative humidity and the films were immediately heated at 200°C for one hour, so that wormlike structures are expected [20]. In the context of a comparative study of films with many different compositions, this procedure is advantageous because film preparation is less time-consuming and fewer experimental parameters need to be considered.

No influence of the aging time of the solutions on the film properties was observed. The case of the vanadium-based solutions was investigated in more detail because Crepaldi et al. [4] have reported that a solution prepared from $VOCl_3$ requires several days to reach equilibrium through an almost complete reduction of V^{5+} to V^{4+}. However, in the present work VCl_4 is used as the source of vanadium and it was found more convenient to prepare a stock solution of VCl_4 in ethanol due to the exothermic character of the reaction. Therefore it comes as no surprise that the major band in the UV-visible spectra of the precursor solutions (SI-2a) corresponds to V^{4+}, with the band maximum at ~760 nm [4]. The solutions with or without lithium have identical spectra and there is no modification of the spectra after aging during one to four days (SI-2b).

3.2. From hybrid film to inorganic film

Transforming hybrid films into inorganic films requires the removal of the organic phase, most often by thermal decomposition of the structuring agent. For each composition investigated here, FT-IR spectra were collected by transmission on films heated to different temperatures. Fig. 1a shows the spectra of the 1Nb-1Li-1EO series. The absorption peaks of the P123 structuring agent (at ~2900 cm^{-1} and ~1100 cm^{-1}) can be detected up to 300°C (5 min) and are no longer visible at 350°C (5 min). These results are in good agreement with the in-situ thermal ellipsometric analysis reported by Bass et al. [22], where pyrolysis of a similar Pluronic structuring agent (F127, EO_{109}-PO_{70}-EO_{109}) was found to occur between 250°C and 380°C with a maximum rate of pyrolysis at 310°C.

In all NbV-based films and in some V-based films the P123 absorption peaks disappear at a significantly lower temperature (200°C, 1h). This phenomenon might be related to the catalytic effect of vanadium for C–H bond activation during alkyl group oxidation [23]. However, the IR spectra of the 1V-yLi-1EO films heated for 1 hour at 200°C (Fig.1b) show that addition of intermediate contents of lithium ($0.33 \leq y \leq 0.83$) seems to prevent the low temperature decomposition of P123. The reason for these (reproducible) results is unclear and may be related to modifications of the coordination between vanadium species and P123. The low temperature P123 decomposition in the Li-richest film (1V-1Li-1EO) is an exception to the trend, although in this particular case it might be linked to the partial crystallization of the film as LiV_2O_5 (see section 3.4.4 and SI-4d).

3.3. Which films are mesoropous?

Removal of the organic structuring agent by an appropriate heat treatment is expected to yield worm-like mesoporous films only if the addition of lithium in the precursor solution did not interfere too much with the EISA mechanism. Due to the low decomposition temperature of P123, most of the films investigated in this section are amorphous so that an absence of mesostructure cannot be due to a crystallization-induced collapse.

Transmission electron microscopy was used to investigate the microstructure of fragments scratched from the films. Micrographs are shown in Fig. 2 and 3 and in SI-3. Wormlike mesoporosity, when present, was characterized by the atmospheric ellipsometry porosimetry (AEP) technique, which provides information on mean pore size, percentage of free porosity and film thickness (Fig.2 and Table 1). Technical details of data treatment are described in the experimental section. Typical graphs of processed results are shown in Fig. 2c, where the adsorption/desorption isotherms display a type IV profile (Brunauer classification [24]) characteristic of mesoporous materials. The accessible porosity is taken equal to the adsorbed volume at a relative pressure close to 1. Different pore size distributions (PSD) are derived from the adsorption and desorption isotherms, as shown in the inset of Fig. 2c. This is commonly observed and is related to the pore shape: the maxima of the adsorption/desorption PSDs correspond to the pore inside diameter and to the size of the pore bottle neck, respectively [25].

In the present study, it is important to compare AEP with TEM because significant porosity and inter-particle voids in the mesoporous range may still be present after the collapse of an interconnected inorganic architecture into unsintered individual particles.

3.3.1. 1Ti-yLi-1EO and 1Nb-yLi-1EO thin films

As reported in Section 3.2, the 1Ti-yLi-1EO and 1Nb-yLi-1EO films must be heated up to 350°C to decompose the structuring agent. At this temperature, only the Li-free 1Ti-0Li-1EO film is crystallized, as anatase TiO_2 (see section 3.4).

Transmission electron micrographs (Fig.2) show that both 1Ti-0Li-1EO and 1Ti-1Li-1EO films display a worm-like mesoporous structure with pore diameters in the 6-8 nm range. AEP results (Fig.2c and Table 1) reveal that the addition of lithium in the precursor solution leads to a slight increase of the pore size and does not significantly affect the percentage of free porosity (~45%). AEP also reveals a strong increase of the film thickness (from 400 to 1050 nm) when lithium chloride is added to the precursor solution. A calculation based on the density of the phases predicts a thickness increase by only ~20 % if the dipped volume of solution were constant, therefore the thickness increase is mainly attributed to the increase in viscosity (from 10.0 cP to 16.5 cP) that leads to a larger volume of solution adhering to the substrate.

All Nb-based films heated to 350°C display a worm-like mesoporous structure (see TEM micrographs in SI-3a). The TEM pore diameter increases (from ~8 to ~11.5 nm) when the lithium content increases, as confirmed by AEP data in Table 1. The origin of this pore size increase remains unclear, because several experimental parameters vary with lithium addition (see SI-1b). Possible hypotheses related to the micelle formation include a swelling effect or an increase of the micelle aggregation number. Table 1 also shows that the film with the largest Li content (1Nb-1Li-1EO) presents an enhanced percentage of free porosity, which might be explained by the larger pores for a similar wall thickness (as judged from the TEM micrographs). The film thickness increases from 130-160 to 315 nm, due to an increase in viscosity from 4.6-4.9 cP to 5.4 cP.

3.3.2. 0.5V-0.5Nb-yLi-1EO and 1V-yLi-zEO thin films

As reported in Section 3.2, the thermal decomposition temperature is as low as 200°C for the 0.5V-0.5Nb-yLi-1EO films and some of the 1V-yLi-zEO thin films. At this temperature, only the vanadium-based films with the largest lithium content (y = 0.67, 0.83, 1) are partially crystallized as LiV_2O_5 (see section 3.4 and SI-4d).

From TEM characterization (Fig.3 and SI-3b) it turns out that only the lithium-free 0.5V-0.5Nb-0Li-1EO displays a well-defined wormlike mesoporosity, which is retained even after heating to 350°C (see AEP results in Table 1).

Both 0.5V-0.5Nb-0.5Li-1EO and 1V-0Li-1EO films show a poorly-defined mesoporosity which collapses in case of heating to 350°C. The general lack of stability of vanadium-based mesoporous films is usually considered to result from the trend of V^{5+} species to form layered structures incompatible with the curvature necessary to achieve mesopores [4]. In the case of the 1V-0Li-1EO film, crystallization at 350°C (see section 3.4.4) may be an additional cause of mesoporosity collapse.

All the other films have featureless micrographs, with the notable exception of the 1V-0.5Li-1EO hybrid film where nanospheres with diameters from 20 to 55 nm are observed (Fig.3d). Since no particles are detected by dynamic light scattering in the precursor solution, the formation of this particular structure must be evaporation-induced. It should be noted that nanospheres are obtained only for this specific set of conditions: lower and higher lithium contents (y = 0.167, 0.33, 0.67, 0.83, 1) or TM/EO molar ratio (z = 0.2, 0.3, 0.5, 1.5) resulted in unstructured films.

3.4. Inorganic network

The results described in section 3.3 reveal that addition of lithium is compatible with formation of worm-like mesoporous films only in the case of the Ti-based and Nb-based films. Key issues involved in the EISA mechanism are (i) the interactions between the metallic cations and the organic moieties and (ii) the degree of condensation of the inorganic network. In the present case, the presence of both transition metal (TM) and lithium ions in the precursor solution also raises the question of the homogeneity of the cationic distribution in the films.

Considering the hydrolysis molar ratio H_2O/TM ~10, interactions of the cations with the ethylene oxide block of P123 are expected to occur by hydrogen bonding with the oxo/hydroxo/aquo ligands of the hydrolyzed metallic cations, as described by Crepaldi et al. [4] for VO_x thin films (see Scheme 1 in [4]). Li^+ has a much lower nominal charge than the nominally 4+ or 5+ Ti, Nb and V ions, but experiments by Ganguly et al. [8] and Schott et al. [9] have demonstrated that complexation occurs between hydrated Li^+ and PEO chains in aqueous solutions, contrary to the case of larger +1-ions such as Na^+ or K^+. Hydrated lithium salts were also found to be able to form lyotropic liquid-crystalline mesophases with a nonionic surfactant containing a PEO block [26]. These literature data indicate that all metallic cations involved in the present work are able to interact with the PEO block and could play a role in the formation of the mesostructure. However, this does not rule out that "competition" between cations could result in inhomogeneous cationic distribution and/or preferential homo-cationic condensation.

In an attempt to gather information about the inorganic network below the crystallization temperature, FT-IR and Raman spectroscopies were used to characterize the amorphous films. However, most of the spectra display peaks which are too broad to obtain information about the metal-oxygen bonds. This is exemplified by the 500-900 cm^{-1} range of the IR spectra of 1Nb-1Li-1EO films (Fig.1a) or by the Raman spectra of the 1Nb-yLi-1EO films heated at 350°C (thin gray curves in Fig.5a). The V-based films are the only ones that show well defined Raman spectra in the amorphous state (see later).

Since characterization of the amorphous films provided little information, X-ray diffraction complemented by Raman spectroscopy was used to identify the first crystalline phase(s) and the temperature at which this first crystallization occurs. In order to minimize cationic "post-homogeneization" by ionic diffusion at high temperature, thin films were usually heated for only 5 minutes in a furnace pre-heated at a nominal temperature. Although not definitely conclusive, these data were used as an indirect indication of the cationic homogeneity in the inorganic network. For example, crystallization of a lithium-free transition metal oxide was considered as an indication of transition metal ion clustering during the inorganic network condensation. When possible, the crystallization temperature was compared with literature data for other sol-gel syntheses of the same compound but the conclusions should be taken with care since the discussion relies on the assumption that phase nucleation depends only on cationic homogeneity.

3.4.1. 1Ti-yLi-1EO thin films

Fig. 4 shows XRD patterns for 1Ti-1Li-1EO films heated at different temperatures. Raman spectra (SI-5a) agree with the XRD results. The first crystallographic reflections appear after 5 minutes at 500°C or 2 hours at 450°C. The three broad peaks to do not allow distinguishing between Li_2TiO_3 and $Li_4Ti_5O_{12}$, two phases with similar layered structures. The film nominal stoichiometry is closer to $Li_4Ti_5O_{12}$, but the narrower peaks at higher temperature show a better agreement with the Li_2TiO_3 reference card (PDF 00-033-0831 [27,28]). Longer heat treatment and/or higher temperature is necessary to initiate the

crystallization of TiO_2 (anatase) as a secondary phase. By comparison, the anatase reflections of the Li-free film (1Ti-0Li-1EO) are already detected after 5 minutes at 400°C (not shown).

The appearance of lithium titanate as the first crystalline phase and the delayed crystallization of anatase both point to a significant intermixture of Ti and Li ions in the inorganic network at the early stages of polymerization. However, Haetge et al. [10] seem to have obtained a more homogeneous cationic distribution since they report crystallization of pure $Li_4Ti_5O_{12}$ at 600°C, without intermediate phases at lower temperatures. The relevant difference in the experimental conditions is likely to be the water content in the precursor solution. In the work of Haetge et al. [10], water was supplied only through the controlled water partial pressure in the atmosphere. On the contrary, in the present work water was added to the precursor solution to reach a H_2O/TM molar ratio ~10. In such conditions, the hydrolyzed titanium species can condense into small oligomeric units [20], which could be responsible for the imperfect cationic homogeneity in the dip coated film. It should however be emphasized that the films studied here have a better homogeneity than usually encountered in sol-gel syntheses of lithium titanate, where strong reflections of TiO_2 anatase appear first and lithium titanate is formed only at higher temperatures (see [29] for a recent example).

3.4.2. 1Nb-yLi-1EO thin films

All Nb-based films are still amorphous after heating to 550°C. After 5 minutes at 600°C, reflections are present in the XRD patterns of all films (SI-4a), with higher intensity for the Li-rich film reflections. The crystallographic phases detected in each film are listed in Table 2 and are in agreement [30,31] with the Raman spectra shown in Fig. 5a. In the case of the 1Nb-0Li-1EO film, the presence of Nb_2O_5 reflections after 5 minutes at 600°C is in good agreement with the thermal analysis results of Lee et al. [32], who report a crystallization temperature of 575°C. On the contrary, 600°C as crystallization temperature of $LiNbO_3$ in the 1Nb-1Li-1EO film is significantly higher than the 200°C-400°C range reported by other authors [33,34]. This suggests that, in the films studied here, diffusion of Li ions had to take place to allow for crystallization, i.e., that the Li-Nb distribution in the as-formed inorganic network was not homogeneous. This hypothesis could neither be supported nor contradicted by the Raman spectra collected at 350°C (thin gray curves in Fig.5a) because the amorphous films display very broad peaks that do not allow to distinguish between amorphous Nb_2O_5 [35] and amorphous $LiNbO_3$ [31].

The film with intermediate Li content (1Nb-0.5Li-1EO) crystallizes as a mixture of Nb_2O_5, $LiNbO_3$ and $LiNb_3O_8$. Since there is no known crystalline phase with a 1:2 Li:Nb molar ratio, a mixture of $LiNbO_3$ and $LiNb_3O_8$ was expected on the basis of the phase diagram [36]. The presence of the Nb_2O_5 phase might therefore be considered as an indication of cationic inhomogeneity but this conclusion must be taken with care in the absence of literature data on the crystallization of $LiNb_3O_8$ from sol-gel precursors.

3.4.3. 0.5V-0.5Nb-yLi-1EO thin films

The Li-free 0.5V-0.5Nb-0Li-1EO film crystallizes as $NbVO_5$ at 520°C, as expected [16]. Addition of lithium to the precursor solutions lowers the crystallization temperature to 500°C (see Table 2 for the list of phases and SI-4b for the XRD patterns). All observed reflections can be indexed as Li-V-O, Li-Nb-O or Nb-V-O phases. In the first crystalline phases of the film with intermediate Li content (0.5V-0.5Nb-0.5Li-1EO), lithium is combined with vanadium whereas niobium is found in a Li-free Nb-rich $Nb_{18}V_4O_{55}$ phase. In the case of the 0.5V-0.5Nb-1Li-1EO film, all first crystalline phases contain lithium and correspond to a mixture of Li-V-O oxides and Li-Nb-O oxides (as confirmed by the Raman spectrum in SI-5b). The complex composition of the films prevents a detailed discussion but it is interesting to note that crystallization of the $LiNbO_3$ phase occurs 100°C lower in the 0.5V-0.5Nb-1Li-

1EO film by comparison with the corresponding Nb-based film (1Nb-1Li-1EO). 500°C is still a higher temperature than the 200°C-400°C range reported by other authors [33,34] for $LiNbO_3$ crystallization, but the decrease from 600°C to 500°C suggests that lithium is more homogeneously distributed in the 0.5V-0.5Nb-1Li-1EO film than in the 1Nb-1Li-1EO film.

3.4.4. 1V-yLi-1EO thin films

By comparison with the Nb-based and NbV-based films, the V-based series crystallize at significantly lower temperatures (250-350°C). The corresponding XRD patterns can be found in SI-4c. The Li-free film crystallizes as V_2O_5 after 5 minutes at 350°C. LiV_2O_5 is the first crystalline phase to appear in the two lithium-containing films, respectively after 5 minutes at 350°C for 1V-0.5Li-1EO and after 5 minutes at 250°C for 1V-1Li-1EO.

IR spectroscopy confirms that the crystallization temperature of the LiV_2O_5 phase decreases with increasing Li content in the film. Fig. 1b displays the IR spectra of 1V-yLi-1EO films heated at 200°C for 1 hour: characteristic absorptions of LiV_2O_5 (V-O-V bending at ~600 cm^{-1} and V=O stretching at 1015 and 942 cm^{-1} [37]) are observed only in the lithium-rich films (y = 0.67, 0.83 and 1). These absorptions coexist or replace the broad V=O absorption at 1000 cm^{-1} that is found in amorphous films.

In the case of the V-based films, the Raman spectra below the crystallization temperature are sufficiently well-defined for identification of characteristic peaks. Fig. 5b displays the Raman spectra of the 1V-0.5Li-1EO after 5 minutes at 250°C and the 1V-1Li-1EO film after 5 minutes at 200°C. The positions of the 3 main peaks of V_2O_5 (see SI-5c for the complete spectrum) are shown as dashed lines to highlight the absence of V_2O_5 in the lithium-containing films. This suggests that lithium and vanadium are intimately mixed in the inorganic network. However, the coexistence of phases with various Li-V molar ratios [38-40] points to a degree of inhomogeneity in the Li-V distribution.

Conclusions

This work investigated the possibility to prepare mesoporous thin films of Li-Ti, Li-Nb, Li-Nb-V and Li-V oxides through a direct sol-gel EISA route by dissolving a lithium salt in the precursor solution. Experimental conditions involved the common Pluronic structuring agent P123 (EO_{20}-PO_{70}-EO_{20}) and a hydrolysis molar ratio H_2O/TM ~10 (TM = Ti,Nb,V), so that interactions of the cations with the ethylene oxide block of P123 are expected to occur by hydrogen bonding with the oxo/hydroxo/aquo ligands of the hydrolyzed metallic cations.

On the whole, success in preparing mesoporous lithium transition metal oxide films through this "direct synthesis" approach follows the same trend as for the synthesis of lithium-free oxides by EISA.

In the case of Ti-based and Nb-based oxide films, addition of lithium to the precursor solution is compatible with the formation of mesoporous films. X-ray diffraction data suggest that there is a significant intermixture of lithium and transition metal ions but that cationic distribution in the inorganic network is not completely homogeneous, so that the formation of a stable network could be due to preferential condensation of the Ti or Nb species.

On the contrary, formation of vanadium oxide mesoporous films is notoriously difficult and addition of lithium appears to have a clearly detrimental effect, even when half of the vanadium is replaced by niobium as a stabilizer. In films containing both vanadium and niobium, the wormlike mesoporosity becomes poorly defined and finally vanishes with increasing Li content. In the case of the V-based films, the lithium-free vanadium oxide film shows hardly any structure and the lithium-containing films display no structure at all (except for the formation of nanospheres for the specific 1V-0.5Li-1EO hybrid film composition). However, crystallization as lithium vanadium oxides without detection of lithium-free

vanadium oxides suggests a good mixing of lithium and vanadium in the inorganic network, although the coexistence of several Li-V-O phases may indicate some inhomogeneity.

In conclusion, this work confirms that the "direct synthesis" approach is worth investigating. In the case of robust network-forming transition metal cations (Ti^{4+} and Nb^{5+}), the EISA mechanism is compatible with lithium addition. Future work might focus on the investigation of cationic homogeneity and its relation with H_2O/TM hydrolysis molar ratio. In difficult cases such as vanadium-based systems, the EISA approach failed and it might be worth trying to combine the direct synthesis with an Evaporation-Induced Micelle Assembly (EIMA) route [41], where micelles are already present in the precursor solutions because the structuring agents are made up of longer polymeric chains with stronger hydrophilic/hydrophobic contrast than Pluronics. Formation of mesostructured hybrid films would then mainly rely on these pre-existent micelles, so that the good mixing of vanadium and lithium would become an advantage instead of a probable obstacle to the efficient condensation of the inorganic network. In all cases (EISA or EIMA), optimization of the films in view of electrochemical characterization will likely benefit from a shift from the Pluronics copolymers to structuring agents with higher decomposition temperature. Indeed, if formation of mesoporous films by "EIMA direct synthesis" with PS-*b*-PEO structuring agents can be achieved, the pore size and wall thickness are expected to be suitable for electrochemical testing, since previous work [13] has shown that lithium-free porous films prepared by EIMA display improved electrochemical capacity performance by comparison with dense films.

Acknowledgments
This work was supported by the Belgian Science Policy (Belgian State) under the Interuniversity Attraction Poles program (INANOMAT-P6/17). N.K. thanks the F.R.S.-FNRS (National Fund for Scientific Research) in Belgium for a research fellowship. The authors thank Olivier Dubreuil for discussion about the atmospheric ellipsometry porosimetry experiments.

References
[1] K. Edström, D. Brandell, T. Gustafsson, L. Nyholm, Electrochem. Soc. Interface 20 (2011) 41-46.
[2] C.J. Brinker, Y. Lu, A. Sellinger, H. Fan, Adv. Mater. 11 (1999) 579-585.
[3] D. Grosso, F. Cagnol, G.J.A.A. Soler-Illia, E.L. Crepaldi, H. Amenitsch, A. Brunet-Bruneau, A. Bourgeois, C. Sanchez, Adv. Funct. Mater. 14 (2004) 309-322.
[4] E.L. Crepaldi, D. Grosso, G.J.A.A. Soler-Illia, P.-A. Albouy, H. Amenitsch, C. Sanchez, Chem. Mater. 14 (2002) 3316-3325.
[5] G.J.A.A. Soller-Illia, C. Sanchez, New J. Chem. 24 (2000) 493-499.
[6] O. Dag, A. Verma, G.A. Ozin, C.T. Kresge, J. Mater. Chem. 9 (1999) 1475-1482.
[7] P. Lightfoot, M.A. Mehta, P. Bruce, Science 262 (1993) 883-885.
[8]R. Ganguly, V.K. Aswal, J. Phys. Chem. B 112 (2008) 7726-7731.
[9]H. Schott, A.E. Royce, S.K. Han, J. Colloid. Interf. Sci. 98 (1984) 196-201.
[10] J. Haetge, P. Hartmann, K. Brezesinski, J. Janek, T. Brezesinski, Chem. Mater. 23 (2011) 4384-4393.
[11] M. Pfanzelt, P. Kubiak, M. Fleischhammer, M. Wohlfahrt-Mehrens, J. Power Sources 196 (2011) 6815-6821.
[12] M. Nakayama, Y. Uchimoto, M. Wakihara, J. Power Sources 146 (2005) 674-677.
[13] N. Krins, J.D. Bass, D. Grosso, C. Henrist, R. Delaigle, E.M. Gaigneaux, R. Cloots, B. Vertruyen, C. Sanchez, Chem. Mater. 23 (2011) 4124-4131.

[14] K. Brezesinski, J. Wang, J. Haetge, C. Reitz, S.O. Steinmueller, S.H. Tolbert, B.M. Smarsly, B. Dunn, T. Brezesinski, J. Am. Chem. Soc. 132 (2010) 6982-6990.
[15] J. Dewalque, R. Cloots, F. Mathis, O. Dubreuil, N. Krins, C. Henrist, J. Chem. Mater. 21 (2011) 7356-7363.
[16] N. Krins, L. Lepot, R. Cloots, B. Vertruyen, Solid State Ionics 180 (2009) 848-852.
[17] C. Boissière, D. Grosso, S. Lepoutre, L. Nicole, A.B. Bruneau, C. Sanchez, Langmuir 21 (2005) 12362-12371.
[18] S.S. Soni, G. Brotons, M. Bellour, T. Narayanan, A. Gibaud, J. Phys. Chem. B 110 (2006) 15157-15165.
[19] D. L. Berthier, I. Schmidt, W. Fieber, C. Schatz, A. Furrer, K. Wong, S. Lecommandoux, Langmuir 26 (2010) 7953-7961.
[20] E.L. Crepaldi, G.J.A.A. Soler-Illia, D. Grosso, F. Cagnol, F. Ribot, C. Sanchez, J. Am. Chem. Soc. 125 (2003) 9770-9786.
[21] P.C.A. Alberius, K.L. Frindell, R.C. Hayward, E.J. Kramer, G.D. Stucky, B.F. Chmelka, Chem. Mater. 14 (2002) 3284-3294.
[22] D. Bass, D. Grosso, C. Boissière, C. Sanchez, J. Am. Chem. Soc. 130 (2008) 7882-7897.
[23] M. Sarzi-Amedè, S. Morselli, P. Moggi, A. Maione, P. Ruiz, M. Devilliers, Appl. Catal. A-Gen. 284 (2005) 11-20.
[24] S. Brunauer, L. Deming, W. Deming, E. Teller, J. Am. Chem. Soc. 62 (1940) 1723-1732.
[25] M. Etienne, A. Quach, D. Grosso, L. Nicole, C. Sanchez, A. Walcarius, Chem. Mater. 19 (2007) 844-856.
[26] C. Albayrak, A. Cihaner, O. Dag, Chem. Eur. J. 18 (2012) 4190-4194.
[27] M. Castellanos, A.R. West, J. Mater. Sci. 14 (1979) 450-454.
[28] International Centre for Diffraction Data, Powder Diffraction File PDF4+ database.
[29] J. Mani, H. Katzke, S. Habouti, K.R. Moonoosawmy, M. Dietze, M. Es-Souni, J. Mater. Chem. 22 (2012) 6632-6638.
[30] N.V. Sidorov, M.N. Palatnikov, V.T. Kalinnikov, Opt. Spectrosc. 82 (1997) 32-38.
[31] P. Heitjans, M. Masoud, A. Feldhoff, M. Wilkening, Faraday Discuss. 134 (2007) 67-82.
[32] B. Lee, T. Yamashita, D. Lu, J.N. Kondo, K. Domen, Chem. Mater. 14 (2002) 867-875.
[33] V. Joshi, M.L. Mecartney, J. Mater. Res. 8 (1993) 2668-2678.
[34] H.C. Zeng, S.K. Tung, Chem. Mater. 8 (1996) 2667-2672.
[35] B. Orel, M. Macek, J. Grdadolnik, A. Meden, J. Solid State Electrochem. 2 (1998) 221-236.
[36] T.A. Rost, H. Lin, T.A. Rabson, R.C. Baumann, D.L. Callahan, J. Appl. Phys. 72 (1992) 4336-4343.
[37] Y.W. Wang, H.Y. Xu, H. Wang, Y.C. Zhang, Z.Q. Song, H. Yan, C.R. Wan, Solid State Ionics 167 (2004) 419-424.
[38] R. Baddour-Hadjean, J.P. Pereira-Ramos, C. Navone, M. Smirnov, Chem. Mater. 20 (2008) 1916-1923.
[39] A. Bouzidi, N. Benramdane, M. Medles, M. Khadraoui, S. Bresson, C. Mathieu, R. Desfeux, M.E. Marssi, J. Alloy. Compd. 503 (2010) 445-448.
[40] G. Yang, G. Wang, W. Hou, J. Phys. Chem. B 109 (2005) 11186-11196.
[41] C. Sassoye, C. Laberty, H.L. Khanh, S. Cassaignon, C. Boissière, M. Antonietti, C. Sanchez, Adv. Funct. Mater. 19 (2009) 1922-1929.

Figures

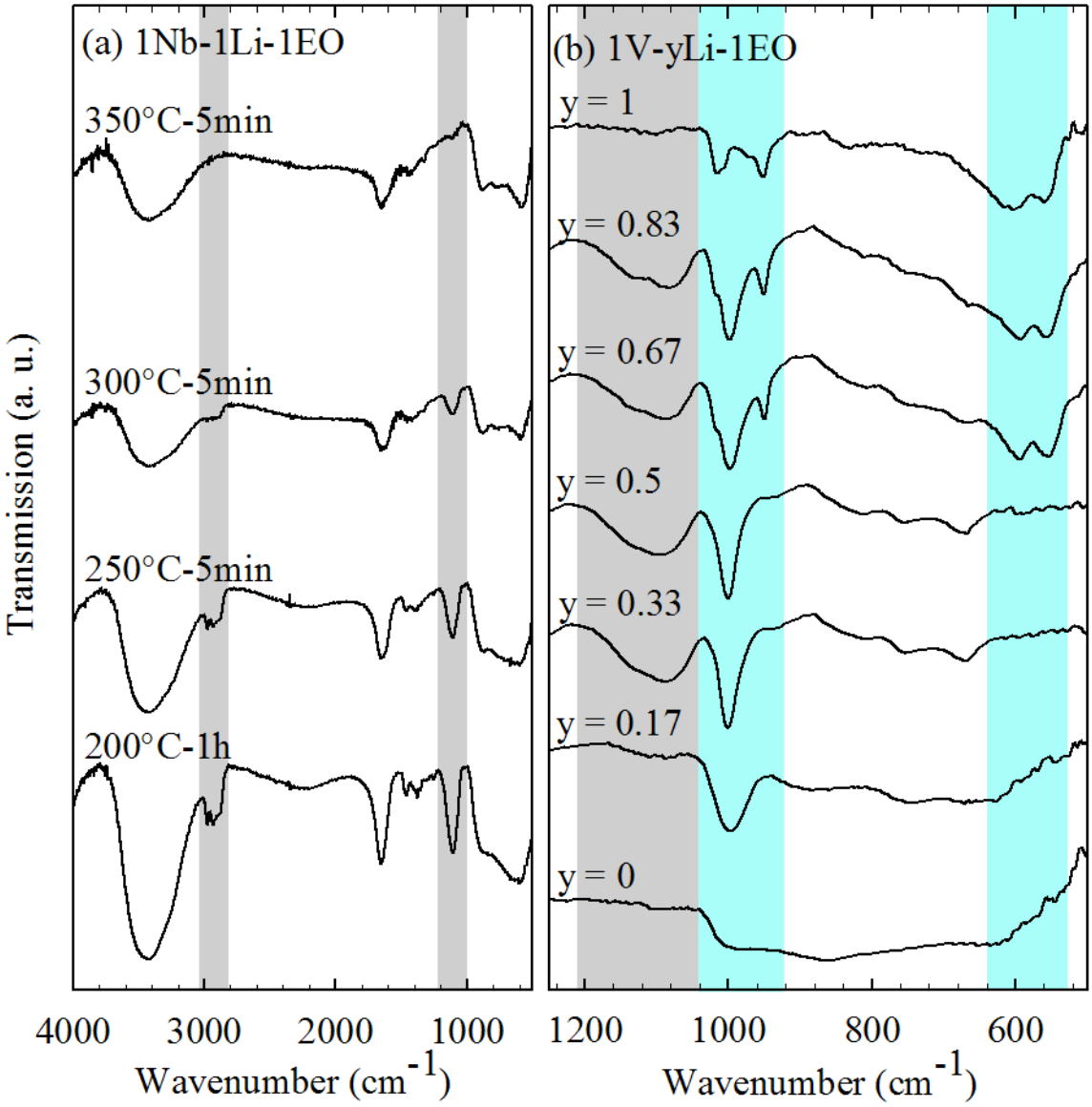

Fig. 1: Transmission IR spectra of (a) 1Nb-1Li-1EO films heated to different temperatures and (b) 1V-yLi-1EO films with different lithium contents, heated at 200°C for 1 hour. In (a) and (b), the positions of the absorption bands corresponding to the structuring agent are highlighted by gray shading and discussed in section 3.2. In (b), the positions of absorption bands corresponding to vanadium-oxygen vibrations are shaded in blue and discussed in section 3.4.4.

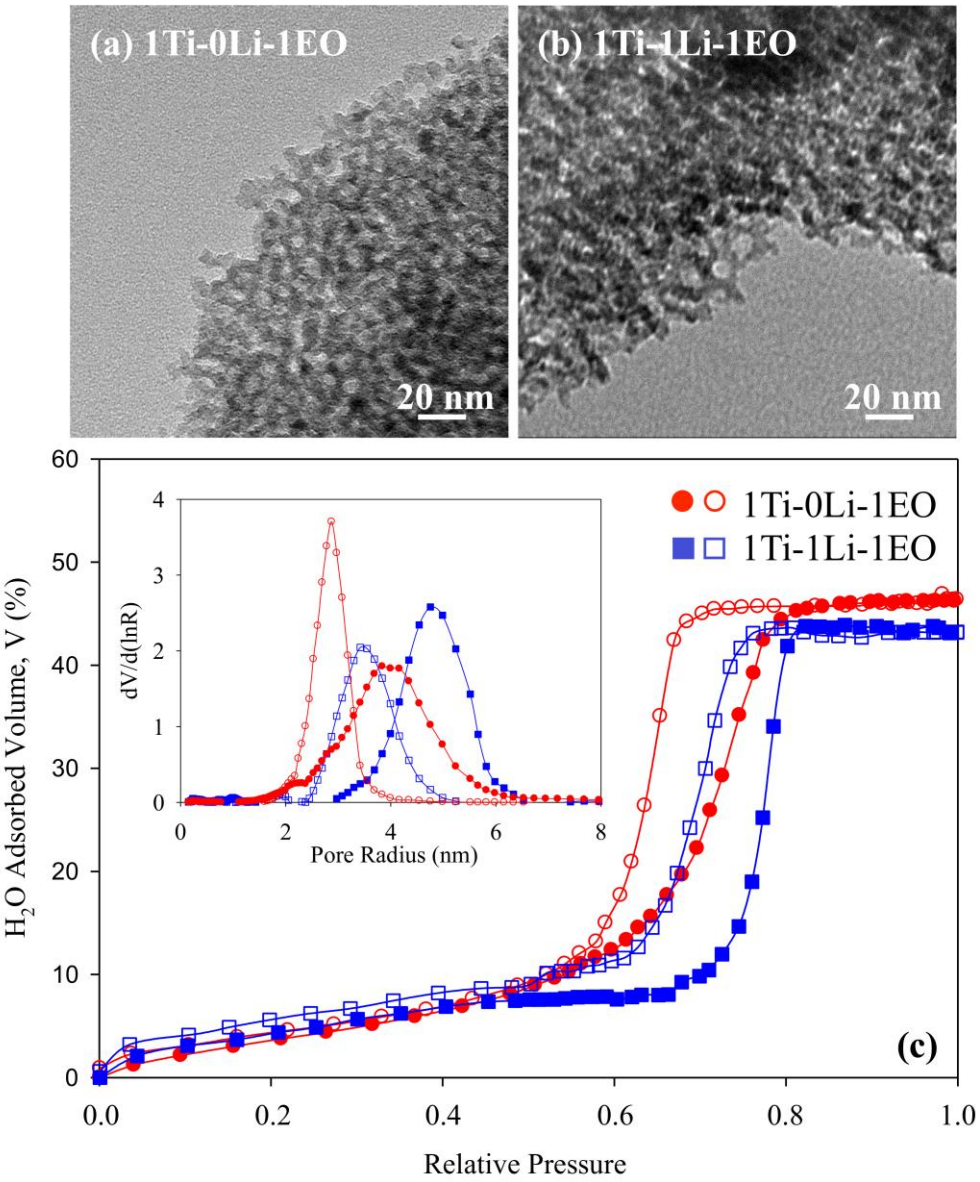

Fig. 2 : TEM micrographs of (a) 1Ti-0Li-1EO and (b) 1Ti-1Li-1EO films calcined at 350°C for 2h and (c) AEP isotherm curves of 1Ti-0Li-1EO and 1Ti-1Li-1EO films heated for 2h at 350°C (full symbols : adsorption, hollow symbols : desorption). Inset: Corresponding pore size distributions.

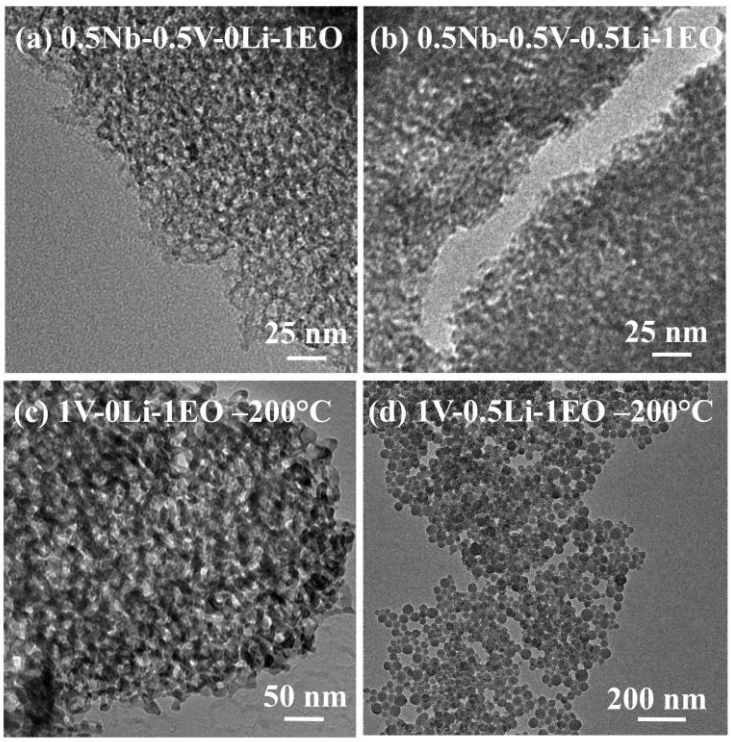

Fig. 3 : TEM micrographs of (a) 0.5Nb-0.5V-0Li-1EO, (b) 0.5Nb-0.5V-0Li-1EO, (c) 1V-0Li-1EO and (d) 1V-0.5Li-1EO films heated for 1 hour at 200°C.

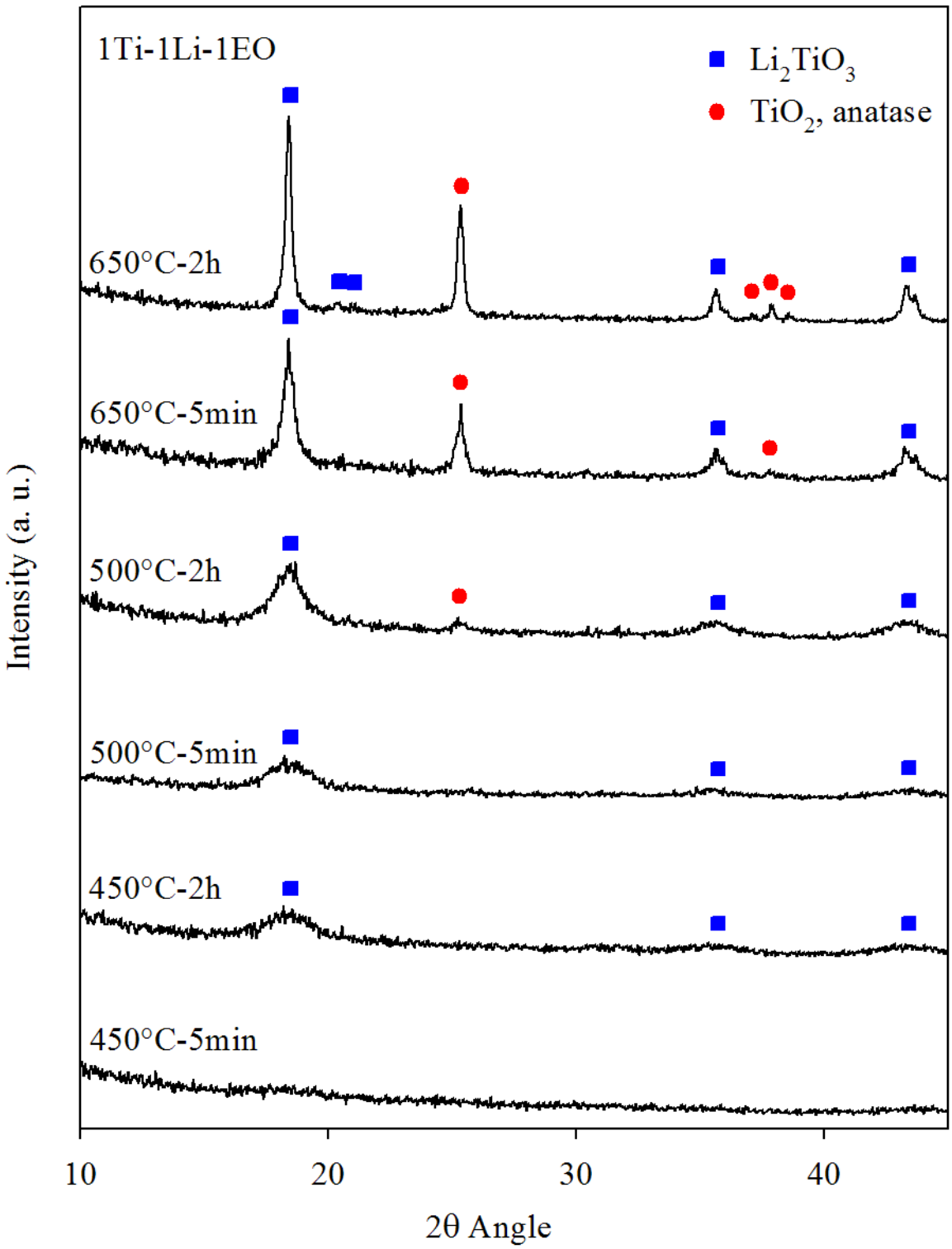

Fig. 4 : XRD patterns of 1Ti-1Li-1EO films heated at different temperatures for 5 minutes or 2 hours.

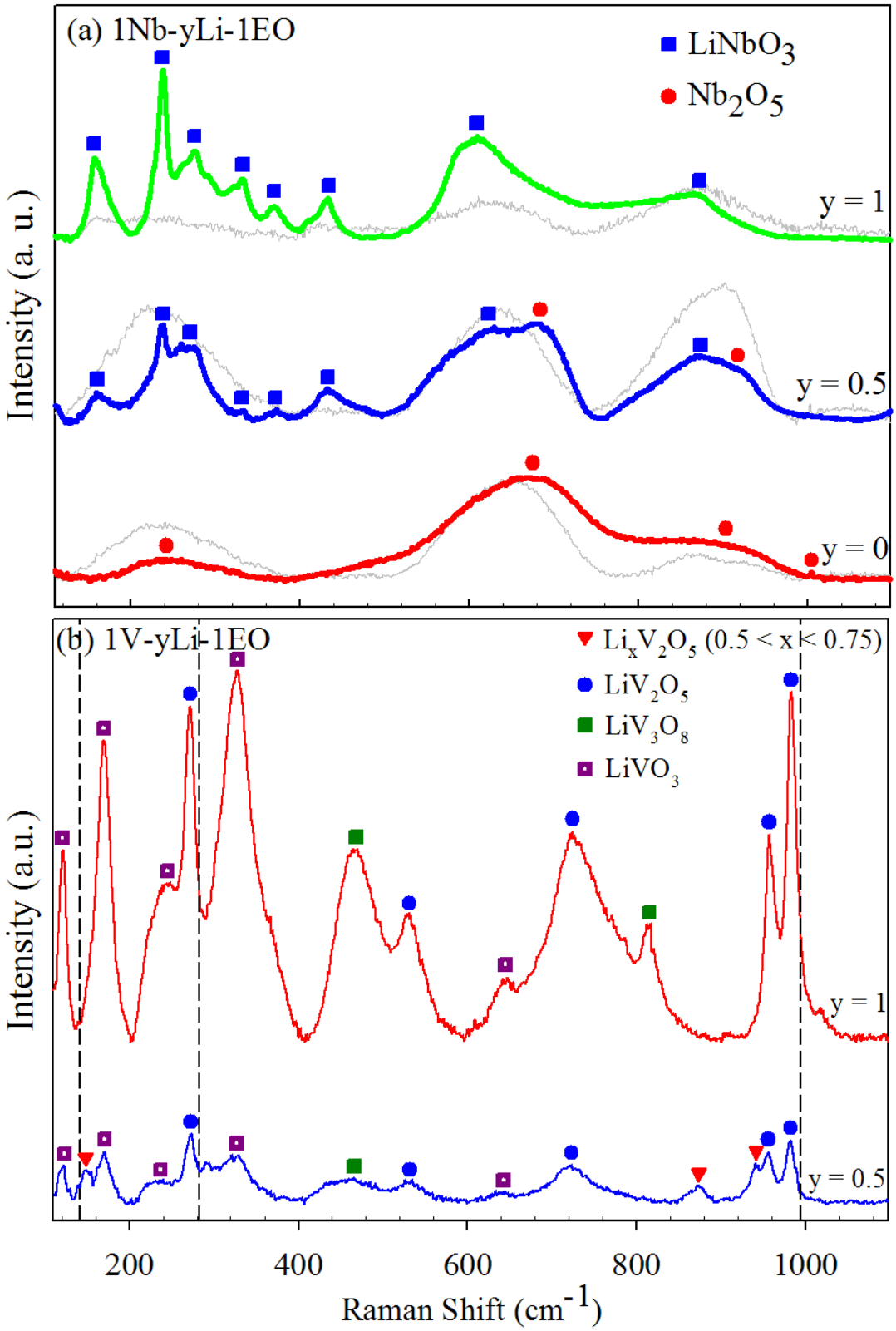

Fig. 5 : Raman spectra of (a) 1Nb-yLi-1EO films calcined at 350°C-5min (thin gray lines) and at 600°C-5min (bold colored lines) and (b) 1V-yLi-1EO calcined at 250°C-5min (y=0.5) and 200°C-5min (y=1). For comparison purposes, dashed lines represent the positions of the major peaks of V_2O_5.